Dynamics Study of the O + HO_2 Reaction Using Two DMBE Potential Energy Surfaces: The Role of Vibrational Excitation†

Dora M. Silveira, Pedro J. S. B. Caridade, and António J. C. Varandas*

Departamento de Química, Universidade de Coimbra, 3004-535 Coimbra, Portugal

Received: January 30, 2004; In Final Form: March 17, 2004

We investigate the effect of vibrational excitation on the dynamics and kinetics of the atmospheric reaction $O(^3P) + HO_2 \rightarrow OH + O_2$ using two double many-body expansion potential energy surfaces previously reported. The results show that such an effect is relatively minor even considering HO_2 with contents of vibrational excitation close to the $H + O_2$ dissociation asymptote. It should therefore not bear drastic implications in atmospheric modeling where such an effect has been ignored thus far.

1. Introduction

The reaction of a oxygen atom with a hydroperoxyl radical both in their ground electronic states is important in the chemistry of the middle atmosphere where it provides a natural odd-oxygen destruction pathway. Moreover, along with the reactions

$$O + OH \rightarrow H + O_2 \quad (1)$$

$$H + O_2 + M \rightarrow HO_2 + M \quad (2)$$

$$H + O_3 \rightarrow OH + O_2 \quad (3)$$

it plays a crucial role in controlling the partitioning among H, OH, and HO_2 radicals.[1] It is therefore not surprising that it has been much studied both experimentally[2−10] and theoretically.[11−13] Despite such an effort, it has been proposed[14] from atmospheric modeling studies that best agreement with observations could be attained only if the recommended rate constant[15] were scaled down by values up to 75% or so. In turn, one of us[16−18] has recently suggested that the internal energy content of O_2, OH, and HO_2 species could not be ignored when discussing the so-called "ozone deficit problem" (refs 16 and 19 and references therein) and "HO_x dilemma"[20] in the middle atmosphere having in mind that situations of local thermodynamic disequilibrium[16,19] are probably the rule rather than the exception at such rarefied regions of the atmosphere.

Due to being a pivotal intermediate in atmospheric chemistry and combustion processes as well as in chemical and biological oxidation, the ground electronic state of HO_3 has been widely studied.[13] Experimentally, measurements of heats of formation have shown that $H^\circ_{298}(HOOO) = -1 \pm 5$ kcal mol^{-1}, which led to the prediction[21,22] that HO_3 should be a relatively stable intermediate species, lying 10 ± 5 kcal mol^{-1} below the HO + O_2 dissociation limit. Neutralization−reionization mass spectrometry experiments by Cacace et al.[23,24] confirmed such a hydrogen trioxide to be stable toward dissociation by 8−10 kcal mol^{-1}, although the barrier could be purely kinetic[24] (experimentally, this implies that HO_3 may still be metastable!). Theoretically, except for a few ab initio calculations,[25−27] most others[28−33] suggest HO_3 to be a metastable species that lies above the OH + O_2 dissociation limit being separated from the products by a small activation barrier. This is the case also for the HO_3 double many-body expansion potential energy surface[33] (heretofore referred to as DMBEI surface), which shows the lowest energy HO_3 structure to be about 2.3 kcal mol^{-1} above the OH + O_2 dissociation limit, with the dissociation proceeding via a loose OH···O_2 transition state with a small activation energy. In fact, such a surface was calibrated at short range from the ab initio unrestricted configuration interaction energies with single-electron and double-electron excitations (UCISD) reported in ref 33, whereas its long-range part includes the electrostatic energy up to four-body terms and the dynamical correlation truncated at the three-body level. More recently,[27] an improved DMBEII surface has been reported based on 5038 QCISD/CBS (quadratic configuration interaction including single and double electron excitations extrapolated to the complete basis set limit) points, which should be accurate in regions of configuration space covering from the HO_3 intermediate up to the OH + O_2 products channel. Such QCISD/CBS[27] calculations predict HO_3 to be stable with a *cis*-HO_3 geometry, although this is only 1.35 kcal mol^{-1} lower than the *trans*-HO_3 isomer.[16]

Although some significant differences are observed[16] in the spectroscopy of the HO_3 intermediate relative to the data reported[34] from measurements of the infrared spectra of HO_3 generated in argon matrixes, they are not expected to play a major role in the kinetics of the reaction $O + HO_2 \rightarrow OH + O_2$ since this is highly exothermic ($\Delta H = -51.94$ kcal mol^{-1}). In fact, dynamics studies of the title reaction carried in the DMBEI potential energy surface employing both classical trajectories[11] and reduced-dimensionality quantum dynamics[12] have shown fairly good agreement between themselves and the available experimental data. A similar trend has been observed for classical[35] and quantum reduced-dimensionality[36] calculations in the $H + O_3$ reaction using DMBEI, as well as for the OH(v') + O_2(v'') reverse reaction using both the DMBEI[37−41] and DMBEII[39] potential energy surfaces; for further details, see ref 16.

In discussing possible clues related to the so-called "ozone deficit problem" and "HO_x dilemma" in the middle atmosphere,[18] we have shown that vibrationally excited HO_2 radicals may be abundant at such altitudes, providing a nonconventional

† Part of the "Gert D. Billing Memorial Issue".

* To whom correspondence should be addressed. E-mail: varandas@qtvs1.qui.uc.pt.

10.1021/jp049575z CCC: $27.50
Published on Web 06/25/2004

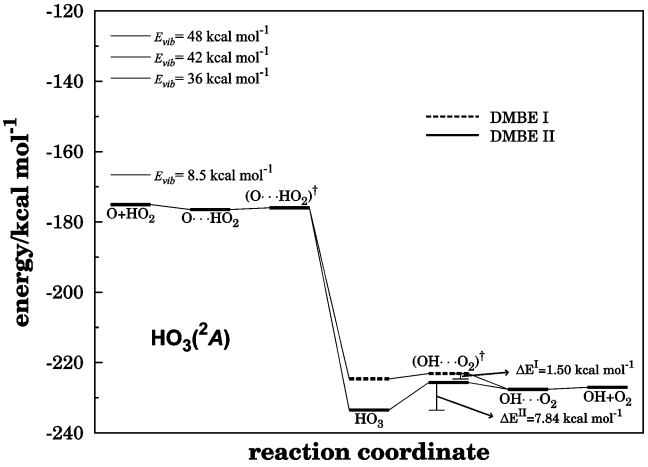

Figure 1. Energetics of the title reaction based on the DMBEI and DMBEII potential energy surfaces. Also indicated by the horizontal lines are the internal energies associated to the various vibrational excitations of H_2O employed in the present work.

source of H atoms and hence a crucial role in the partitioning of odd-hydrogen species. The relevant question would then be how much do such vibrationally excited hydroperoxyl radicals affect the rate constant of the O + HO_2 reaction. It is an answer to this critical question that we attempt in the present work by running trajectories on the realistic DMBEI and DMBEII potential energy surfaces. Although quantum effects are ignored, previous work[12,13] suggests that they should have no drastic effect.

The paper is organized as follow. In section 2, we summarize the essential features of the two potential energy surfaces utilized in the present work, whereas the trajectory calculations are described in section 3. This includes a brief summary of the methodology in subsection 3.1, and the discussion of the results in subsection 3.2. The conclusions are in section 4.

2. Potential Energy Surfaces

A detailed comparison of the two DMBE potential energy surfaces has been reported elsewhere,[16] and hence, we focus here on their essential features. Figure 1 summarizes the energetics of the title reaction based on the DMBEI and DMBEII potential energy surfaces. Although the values of some numerical coefficients in the four-body extended Hartree−Fock energy added in ref 27 have been slightly changed to avoid instabilities in some of the trajectories (due to a drastic but continuous variation of the energy), the implications are minor, and hence, we maintain the denomination of DMBEII for the current working version (this may be obtained from the corresponding author upon request). In fact, the differences are negligibly small as can be assessed by comparing the values indicated in Figure 1 with those of the corresponding plot in ref 16. Furthermore, a comparison of the energetic and geometric attributes of this slightly modified version of DMBEII are reported in Table 1 and compared with the original values.[27] Note that the differences between the original and modified forms are probably within the error of the ab initio calculations from which the DMBEII surface has been modeled. Note especially that the saddle point for reaction occurs after the small O···HO_2 van der Waals minimum but below the energy of reactants. Thus, one expects long range forces to dictate the course of reaction especially at low collision energies such as those of relevance in the middle atmosphere.

Figure 2 shows a perspective view/contour plot for the reaction O + HO_2 → OH + O_2 based on the DMBEI potential energy surface, with a similar one being shown in Figure 3 for DMBEII. The notable feature is the minimum which in DMBEII represents a stable structure while in DMBEI corresponds to a metastable one which lies above the OH + O_2 asymptote. As

TABLE 1: Geometrical and Energetic Attributes of Most Important Features in DMBEI and DMBEII Potential Energy Surfaces

property	DMBE I	DMBE II[a]	
	HO_3 Minimum		
R_{HO_a}/a_0	1.8964	1.8440	(1.8468)
$R_{O_aO_a}/a_0$	2.9446	2.7880	(2.7914)
$R_{O_aO_a}/a_0$	2.3311	2.3778	(2.3793)
$\angle HO_aO_c$/deg	96.3	97.8	(97.7)
$\angle O_aO_bO_d$/deg	113.5	110.4	(110.2)
$\angle HO_aO_bO_c$/deg	90.6	0.0	(0.0)
energy/E_h	−0.3580	−0.3717	(−0.3721)
	HO···O_2−TS		
R_{HO_a}/a_0	1.9491	1.8106	(1.8119)
$R_{O_aO_b}/a_0$	3.3073	3.4817	(3.4927)
$R_{O_bO_c}/a_0$	2.3897	2.3092	(2.3069)
$\angle HO_aO_c$/deg	94.6	98.7	(98.8)
$\angle O_aO_bO_d$/deg	118.7	125.7	(125.4)
$\angle HO_aO_bO_c$/deg	82.9	0.0	(0.0)
energy/E_h	−0.3556	−0.3597	(−0.3596)

[a] The numbers refer to the current working version, with those in parentheses corresponding to the originally published ones.[27]

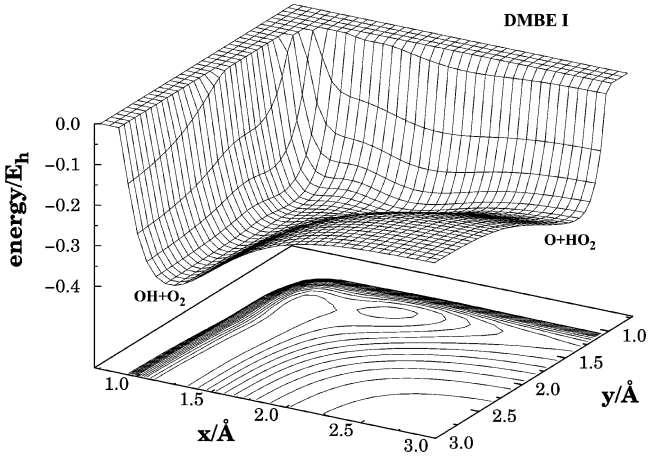

Figure 2. Perspective view/contour plot for the reaction O + H_2O → OH + O_2 based on the DMBEI potential energy surface. The ∠OOO and ∠HOO angles as well as the torsion angle ∠HOOO and the H−O distance are partially relaxed (112.7 ≤ ∠HOO° ≤ 104.3, 82.6 ≤ ∠HOOO° ≤ 90.6, 0.9708 ≤ R_{OH}/Å ≤ 1.0315). Contours start at $-0.3618E_h$, with an equal spacing of 16 mE_h.

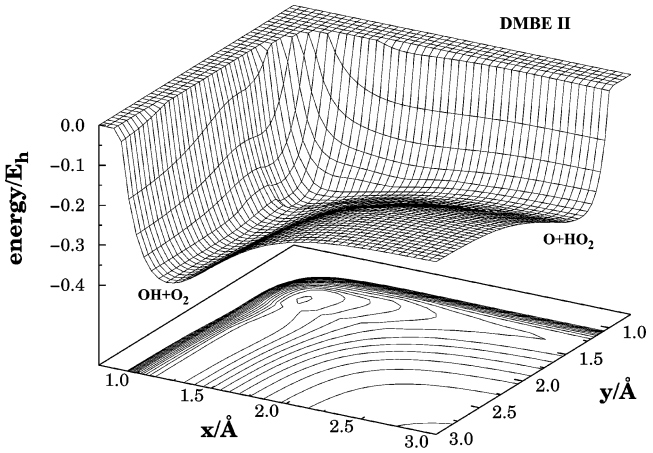

Figure 3. As in Figure 2 but for the DMBEII potential energy surface utilized in the present work.

TABLE 2: Summary of the Dynamics Results for DMBEI

E_{vib}/ kcal mol^{-1}	E_{tr}/ kcal mol^{-1}	b_{max}/ Å	N_t	P_r/% eq 6	eq 7	eq 5	$\sigma^r \pm \Delta\sigma^r$/ Å^2
8.5	0.1	8.1	500	86.0	1.0	1.2	177.26 ± 3.20
	0.5	6.0	500	75.6	0.8	0.8	85.50 ± 2.17
	1.0	5.4	500	70.4	1.4	0.6	64.49 ± 1.87
	2.0	4.7	500	65.8	1.6	1.2	45.66 ± 1.47
	4.0	4.2	500	62.8	2.0	1.0	34.80 ± 1.20
	6.0	4.0	500	67.0	1.8	1.2	33.68 ± 1.06
	8.0	3.9	500	61.6	2.4	0.2	29.43 ± 1.04
	12.0	3.7	500	60.2	1.4	0.6	25.89 ± 0.94
	16.0	3.6	500	58.2	2.0	1.0	23.70 ± 0.90
36.0	0.1	8.2	500	82.4	4.2	11.4	174.06 ± 3.60
	0.5	6.1	500	76.8	4.2	6.0	89.78 ± 2.21
	1.0	5.5	1000	67.2	2.0	5.6	63.86 ± 1.41
	2.0	4.6	1000	66.4	2.8	4.2	44.07 ± 0.99
	4.0	4.2	1000	66.8	2.7	3.8	37.02 ± 0.83
	6.0	4.1	500	62.6	2.4	3.4	33.06 ± 1.14
	8.0	3.9	500	61.0	2.4	0.2	29.15 ± 1.04
	12.0	3.7	500	64.4	4.0	4.2	27.70 ± 0.92
	16.0	3.7	500	57.0	2.0	1.0	24.51 ± 0.95
42.0	0.1	8.1	500	80.2	6.2	38.0	165.31 ± 3.67
	0.5	6.1	500	74.0	4.4	33.6	86.51 ± 2.29
	1.0	5.3	1000	69.3	5.7	29.6	61.16 ± 1.29
	2.0	4.6	1000	68.8	3.8	16.0	45.74 ± 0.97
	4.0	4.3	1000	61.1	4.2	21.9	36.65 ± 0.89
	6.0	4.1	500	60.2	4.6	20.0	31.79 ± 1.16
	8.0	4.0	500	59.6	5.0	19.2	29.96 ± 1.10
	12.0	3.9	500	56.2	5.2	16.2	26.85 ± 0.96
	16.0	3.7	500	55.8	4.6	14.6	24.00 ± 0.96
48.0	0.1	8.2	500	76.6	10.8	32.8	161.81 ± 4.00
	0.5	6.1	500	74.2	10.6	31.6	86.74 ± 2.29
	1.0	5.4	1000	61.2	11.0	28.2	65.23 ± 1.31
	2.0	4.7	1000	68.4	10.2	29.5	47.47 ± 1.02
	4.0	4.5	1000	54.9	5.0	22.3	34.93 ± 1.00
	6.0	4.2	500	57.6	6.6	23.4	31.92 ± 1.22
	8.0	4.3	500	52.8	6.4	19.6	30.67 ± 1.30
	12.0	4.2	500	47.3	6.0	17.2	26.21 ± 0.94
	16.0	4.1	500	45.0	8.4	14.6	23.76 ± 1.17

TABLE 3: Summary of the Dynamics Results for DMBEII

E_{vib}/ kcal mol^{-1}	E_{tr}/ kcal mol^{-1}	b_{max}/ Å	N_t	P_r/% eq 6	eq 7	eq 5	$\sigma^r \pm \Delta\sigma^r$/ Å^2
8.5	0.1	8.1	500	73.4	0.2	0.2	151.29 ± 4.07
	0.5	6.0	500	59.0	0.0	0.0	66.73 ± 2.49
	1.0	5.1	500	53.4	0.0	0.4	43.63 ± 1.82
	2.0	4.4	500	57.2	0.0	0.4	34.79 ± 1.35
	4.0	3.9	500	59.0	0.0	0.2	28.19 ± 1.05
	6.0	3.7	500	59.8	0.8	0.4	25.72 ± 0.94
	8.0	3.5	500	59.8	0.8	0.6	23.01 ± 0.84
	12.0	3.5	500	56.0	1.4	0.4	21.55 ± 0.85
	16.0	3.4	500	56.2	0.8	1.4	20.41 ± 0.81
36.0	0.1	8.1	500	76.6	0.4	0.2	157.89 ± 3.90
	0.5	6.0	500	65.2	0.0	0.2	73.74 ± 2.41
	1.0	5.2	500	58.0	0.0	0.4	50.97 ± 1.86
	2.0	4.6	500	55.8	0.6	0.4	36.83 ± 1.48
	4.0	4.2	500	53.6	0.2	0.8	29.70 ± 1.24
	6.0	3.9	500	55.4	2.0	0.6	26.47 ± 1.06
	8.0	3.8	500	55.6	1.2	1.4	25.22 ± 1.01
	12.0	3.7	500	51.8	2.0	1.0	22.28 ± 0.96
	16.0	3.6	500	52.4	2.6	1.6	21.33 ± 0.91
42.0	0.1	8.1	500	74.4	1.6	13.2	152.53 ± 4.04
	0.5	6.0	500	78.8	1.4	6.4	73.29 ± 2.42
	1.0	5.1	500	63.6	3.0	5.8	51.97 ± 1.76
	2.0	4.6	500	55.8	1.0	3.6	38.82 ± 1.47
	4.0	4.2	500	57.2	2.4	4.0	31.92 ± 1.22
	6.0	3.9	500	53.0	2.2	3.4	25.33 ± 1.07
	8.0	3.8	500	56.0	3.4	4.8	25.40 ± 1.01
	12.0	3.7	500	56.4	5.2	16.2	24.26 ± 0.95
	16.0	3.7	500	52.0	3.6	4.8	22.36 ± 0.96
48.0	0.1	8.1	500	75.4	4.8	35.0	155.41 ± 3.97
	0.5	6.1	500	66.4	3.2	29.8	77.62 ± 2.47
	1.0	5.2	500	59.2	4.2	26.4	50.29 ± 1.87
	2.0	4.5	500	65.0	5.2	28.0	41.35 ± 1.36
	4.0	4.2	500	56.6	5.2	21.8	31.37 ± 1.23
	6.0	4.0	500	59.8	4.6	23.6	30.06 ± 1.10
	8.0	3.9	500	55.8	4.2	21.4	27.91 ± 1.05
	12.0	3.8	1000	54.4	5.6	15.6	24.68 ± 1.01
	16.0	3.6	500	58.4	4.0	18.2	23.78 ± 0.98

noted in ref 27, the topography of the two surfaces is very similar at other regions of the molecule configuration space, as indeed may be verified by looking at other cuts of the potential energy surface. For example, a plot similar to Figure 3 of ref 11 cannot be distinguished by naked eye for the two DMBE surfaces and, hence, will not be reported. We also recall that, for the attacking oxygen atom moving coplanarly around the equilibrium HO_2 target molecule, the potential energy surface is in both cases purely attractive when the oxygen atom attacks the molecule along certain nonlinear paths, whereas the remaining directions offer significant barriers before it gets near the molecule. Such a barrierless optimum reaction path is in agreement with the ab initio Hartree−Fock MC(DZP) calculations of Dupuis et al.[25] but for a normal approach. However, the disagreement with the ab initio calculations in predicting a coplanar barrier for the O + HO_2 (and H + O_3) channels should not be overemphasized, since the picture may drastically change upon use of more complete one electron basis sets and inclusion of full dynamical correlation. Both DMBE surfaces also predict the direct abstraction of the hydrogen atom to involve a high activation energy, and hence, it is highly unlikely at low energies. For future reference, we indicate also in Figure 1 the energies associated to the various vibrational energies of HO_2 employed in the present work.

3. Trajectory Calculations

3.1. Methodology and Technical Details. Following previous work,[35] we have employed the QCT method as implemented in the MERCURY/VENUS[42] codes, suitably adapted to study the title collisional processes. The initial conditions were defined by using the standard fixed normal mode sampling procedure.[42] Needless to say, the normal mode sampling is an approximate method due to the significant anharmonicity of the HO_2 potential energy surface. Specifically, besides considering HO_2 in its ground vibrational state (E_{vib} = 8.5 kcal mol^{-1}), we have also considered triatomic vibrational energies of 36.0, 42.0, and 48.0 kcal mol^{-1} which were democratically distributed by the three vibrational normal modes. In all cases, the rotational energy about each principal axis of inertia of the triatomic has been taken as $k_BT/2$, whereas the rotational temperature has been assumed to be 300*K*. Calculations have been carried out for atom-triatom translational energies over the range $0.1 \le E_{tr}$/ kcal mol$^{-1} \le 16$, as summarized in Table 2 for DMBEI and Table 3 for DMBEII (for reproducibility, all cross sections are quoted with two decimal figures). An optimum step-size for numerical integration of 2.5×10^{-16} s has been chosen, which warrants conservation of the total energy to better than 2 parts in 10^5. Further care has been put on this issue by employing a physically soundful model to extrapolate the cross section to low translational energies (i.e., to represent the excitation function). In all cases, the initial atom−diatomic separation has been fixed at 9 Å such as to warrant that the interaction is essentially negligible at the starting point. To select the maximum value of the impact parameter (b_{max}) which leads to reaction, we have run as usual batches of 50 trajectories for fixed values of *b*. Batches of 500 up to 1000 trajectories have then been carried out for each translational energy (E_{tr}) and initial vibrational energy of HO_2 making a total of 4×10^5 trajectories.

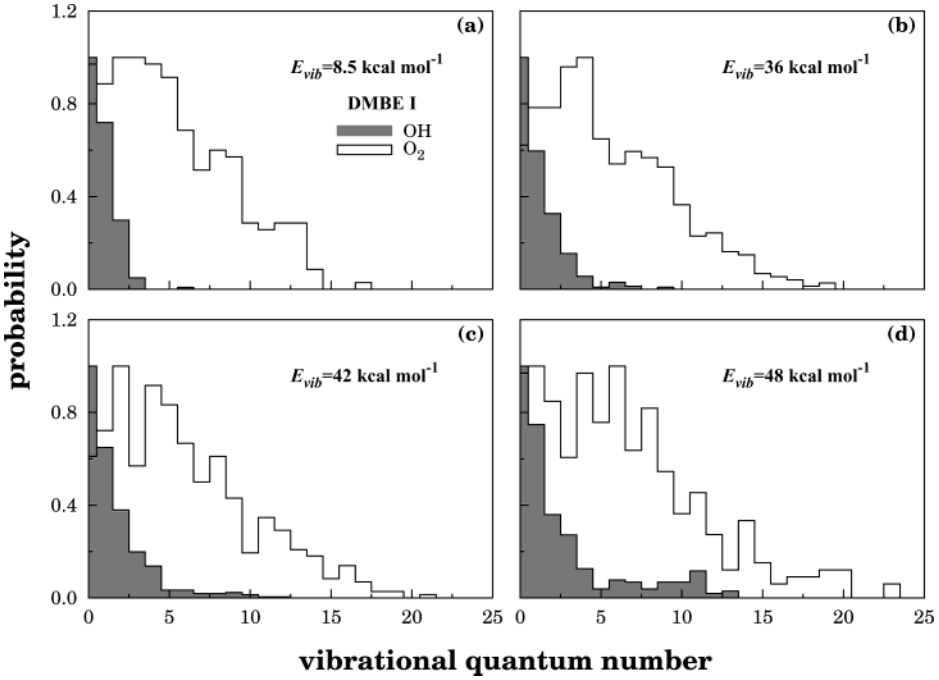

Figure 4. Distributions of vibrational quantum numbers in the products of the $O + HO_2 \rightarrow OH + O_2$ reaction for the DMBEI potential energy surface.

TABLE 4: Energy Partition (in Percent) for the Various Degrees of Freedom in the Products at E_{tr} = 1 kcal mol^{-1}

E_{vib}	$\langle f_{vib}^{O_2} \rangle$			$\langle f_{rot}^{O_2} \rangle$			$\langle f_{vib}^{OH} \rangle$			$\langle f_{rot}^{OH} \rangle$			$\langle f_{trans} \rangle$		
kcal mol^{-1}	eq 6	eq 7	eq 5	eq 6	eq 7	eq 5	eq 6	eq 7	eq 5	eq 6	eq 7	eq 5	eq 6	eq 7	eq 5
DMBE I															
8.5	28.18	0.22	0.32	14.84	0.13	0.23	9.96	0.12	0.63	11.39	0.12	0.19	32.78	0.26	0.62
36.0	26.92	1.94	0.44	12.89	1.07	0.23	6.91	1.94	0.44	10.39	0.58	0.64	29.30	2.31	0.50
42.0	12.95	12.05	1.06	7.57	6.26	0.54	6.50	5.92	3.61	5.72	4.86	1.22	16.31	13.61	1.79
48.0	13.38	10.51	0.97	5.41	6.16	0.50	6.13	5.54	9.81	5.95	5.68	2.05	12.83	13.34	1.73
DMBE II															
8.5	33.64	0.33		13.98	0.03		14.67	0.13		9.61	0.06		27.35	0.20	
36.0	34.59	0.38		13.89	0.03		14.95	0.02		10.26	0.01		25.62	0.26	
42.0	28.59	2.46	0.72	11.86	1.17	0.11	15.21	2.15	2.22	8.03	0.76	0.67	22.46	2.56	1.00
48.0	16.21	15.10	0.69	5.92	5.52	0.24	8.89	8.11	4.00	5.04	4.85	1.10	12.24	11.00	1.06

For a specified translational energy, reactive probabilities (P_r), reactive cross sections, and associated 68% uncertainties (denoted σ_r and $\Delta\sigma_r$, respectively) have been calculated. From the cross sections and by assuming a Maxwell−Boltzmann distribution over the translational energy, the specific thermal rate coefficients can be obtained as

$$k(T) = g_e(T)\left(\frac{2}{k_B T}\right)^{3/2}\left(\frac{1}{\pi\mu}\right)^{1/2}\int_0^\infty E_{tr}\,\sigma_r \exp\left(-\frac{E_{tr}}{k_B T}\right) dE_{tr} \quad (4)$$

where $g_e(T)$ is the electronic degeneracy factor which corresponds to the ratio of the electronic partition functions, k_B is the Boltzmann constant, μ is the reduced mass of the colliding species, and T is the temperature.

3.2. Results and Discussion. Two possible mechanisms can be offered to explain the title reaction

$$O_a + HO_bO_c \rightarrow O_aH + O_bO_c \quad (5)$$

$$O_a + HO_bO_c \rightarrow O_bH + O_aO_c \quad (6)$$

where the indices a, b, and c label the three different oxygen atoms. In fact, the barrier for attacking the middle oxygen atom in HO_2 is high, and hence, the possibility of reaction to occur via

$$O_a + HO_bO_c \rightarrow O_aO_b + HO_c \quad (7)$$

is negligibly small for many translational energies of interest in the present work, except for high vibrational excitations of the reactant HO_2 radical. Note that the classical barrier height for the isomerization $HO_bO_c \leftrightarrow HO_cO_b$ is 40.7 kcal mol^{-1}, and hence, the attack to the O_b atom may occur for high vibrational excitations via the terminal oxygen atom of the HO_cO_b isomer. Thus, eq 3 corresponds to a hydrogen-atom abstraction mechanism, whereas eq 3 refers to a typical oxygen-atom abstraction. Although both mechanisms have been advanced,[43] the kinetic measurements[6,8,9] suggest that the title reaction should occur preferentially via the oxygen-atom abstraction. In fact, this mechanism has been confirmed experimentally[44] via $^{16}O/^{18}O$ substitution and theoretically by our previous calculations.[11]

3.2.1. Products Energy Partitioning. We now examine how the energy is distributed among the two product molecules. Table 4 shows a detailed distribution per channel. It reveals that the dominant contribution comes from the attack of the terminal oxygen atom in HO_2 for the whole range of vibrational excitations considered in the present work, irrespective of the potential energy surface. It also shows that the largest fractions

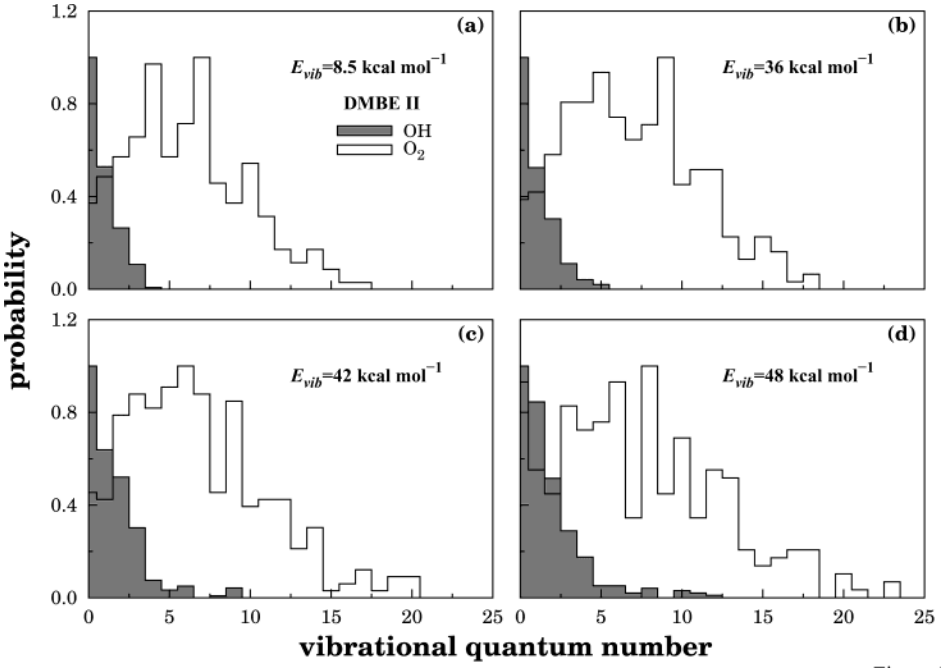

Figure 5. As in Figure 4 but for the DMBEII potential energy surface.

TABLE 5: Vibrational and Rotational Properties of the Product O_2 and OH Molecules at E_{tr} = 1 kcal mol^{-1}

E_{vib}/kcal mol^{-1}	$v^{O_2}_{max}$	$\langle v^{O_2}\rangle$	v^{OH}_{max}	$\langle v^{OH}\rangle$	$j^{O_2}_{max}$	$\langle j^{O_2}\rangle$	$\langle T^{O_2}_{rot}\rangle$/K	j^{OH}_{max}	$\langle j^{OH}\rangle$	$\langle T^{OH}_{rot}\rangle$/K
					DMBE I					
8.5	17	3.91	6	0.73	115	49.52	5175	16	6.88	1475
36.0	19	4.27	9	1.06	137	50.56	5392	17	7.23	1619
42.0	21	3.86	12	1.46	119	52.70	5854	18	7.55	1756
48.0	23	3.75	13	2.45	119	49.10	5088	24	8.55	2222
					DMBE II					
8.5	17	5.99	4	0.73	111	49.52	5175	14	6.55	1345
36.0	18	6.88	5	0.87	121	51.58	5610	16	6.93	1495
42.0	20	6.66	9	1.42	133	51.70	5636	16	6.92	1491
48.0	23	7.25	12	1.69	133	49.88	5250	28	7.86	1894

go to vibrational energy of the newly formed O−O bond and to translational energy, although in both cases their importance slightly diminishes with increasing vibrational excitation of the HO_2 reactant. However, it is possibly more relevant to look to the changes occurring on the three reaction channels taken together. It is then interesting to observe that in DMBEI the decrease on the fraction of vibrational energy in the newly formed O_2 molecule is only of 4% for an increase in the initial vibrational energy content of HO_2 of about 40 kcal mol^{-1}. Such a decrease, if any at all, is even more minute in the case of DMBEII. Since rather small decreases in the fraction of translational energy are also observed with increasing vibrational excitation, one is led to expect that the changes will arise mainly in the fraction of rotational energy (of both O_2 and OH) and vibrational energy of OH. In fact, hardly any noticeable change is seen in the fraction of rotational energy of both O_2 and OH, which leaves the more significant changes for the vibrational energy of the "unbroken" OH bond. As shown from Table 4, such a fraction nearly doubles when going from E_{vib} = 8.5 kcal mol^{-1} to E_{vib} = 48.0 kcal mol^{-1} in the case of DMBEI, with the multiplying factor being roughly 1.5 for the DMBEII results. Such an increase in the vibrational excitation of OH may indeed be attributed to the fact that reaction channels (5) and (7) become open for large values of internal vibrational excitation of HO_2. In fact, a careful examination of all asymptotic channels has shown that some of the hydroxyl radicals correspond to newly formed OH bonds with an appreciable content of vibrational excitation.

We conclude this subsection by examining the distributions of vibrational and rotational quantum numbers in the products. The data are shown graphically in Figures 4 and 5 for the distributions of vibrational quantum numbers obtained for DMBEI and DMBEII, respectively. The maximum and averaged quantum numbers of such distributions are gathered in Table 5. The salient feature from Figures 4 and 5 is that O_2 shows an inverted population peaking at a value of v^{O_2} in the range 2−5 for DMBEI and 4−8 for DMBEII. This is reflected on the averaged vibrational quantum number in the product O_2 molecules which is about $\langle v^{O_2}\rangle$ = 4 for DMBEI and $\langle v^{O_2}\rangle$ = 6−7 for DMBEII. Note that there is only a small variation in $\langle v^{O_2}\rangle$ in going from E_{vib} = 8.5 kcal mol^{-1} to E_{vib} = 48.0 kcal mol^{-1}, both for DMBEI and DMBEII. The same trend is observed for the maximum populated vibrational quantum number which varies for both surfaces between $v^{O_2}_{max}$ = 17 at E_{vib} = 8.5 kcal mol^{-1} and $v^{O_2}_{max}$ = 23 at E_{vib} = 48.0 kcal mol^{-1}. Conversely to the newly formed O_2 molecules which are found to be vibrationally hot, the OH radicals are formed generally vibrationally cold except for the highest vibrational excitations of the reactant HO_2 radical where the maximum populated vibrational quantum number may reach values as large as v^{OH}_{max} = 13. Clearly, for such high vibrational excitations of HO_2, the OH bond may no longer be a "spectator" (as for the lowest vibrational excitations of HO_2) but correspond to a newly formed species since the attack can in this case occur either to the central oxygen atom of HO_2 or to its terminal hydrogen atom. Of

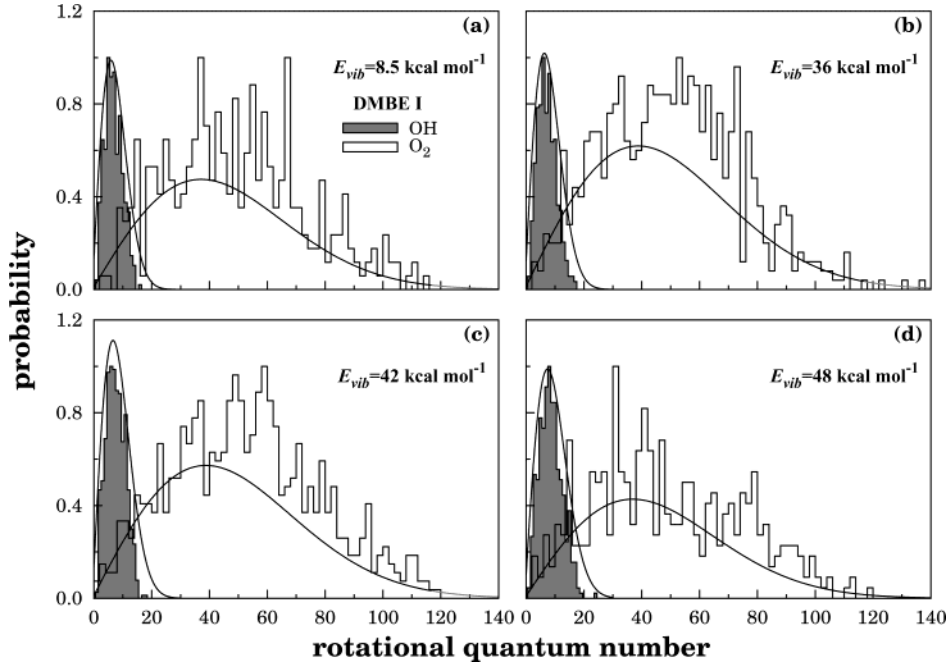

Figure 6. Distributions of rotational quantum numbers in the products of the reaction $O + HO_2 \rightarrow OH + O_2$ for the DMBEI potential energy surface.

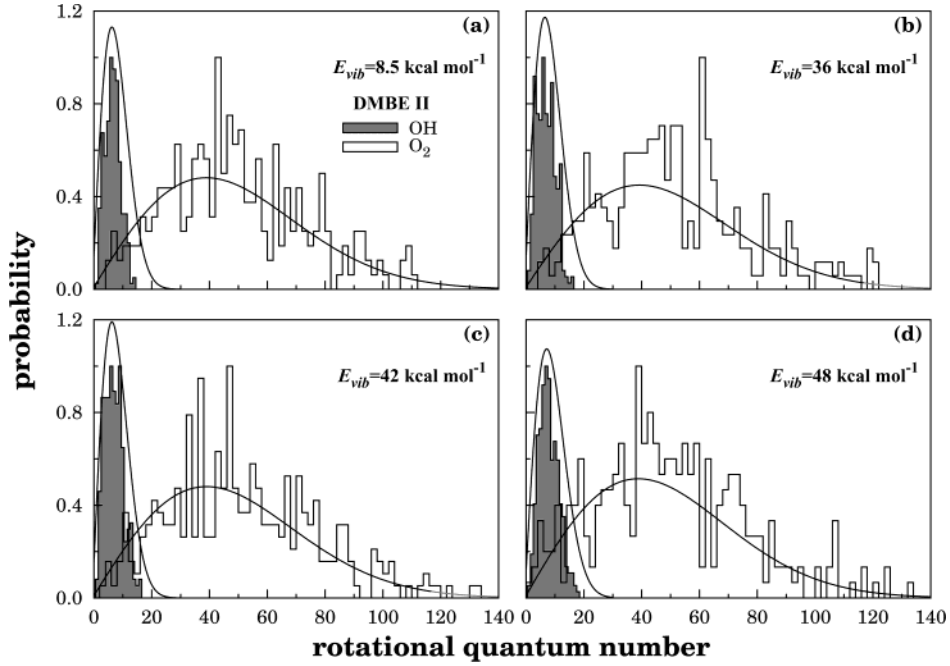

Figure 7. As in Figure 6 but for the DMBEII potential energy surface.

course, as discussed above, HO_2 may isomerize above 40.7 kcal mol^{-1}, and hence, the notion of the central oxygen atom is questionable. Such mechanisms have been verified by careful analysis of a series of trajectories; see also, from Tables 2 and 3, the drastic increase in the cross section when the vibrational excitation reaches 42 kcal mol^{-1}. In fact, one observes that the newly formed hydroxyl radicals can appear with vibrational quantum numbers higher than $v = 9$, especially when the oxygen atom attacks directly the terminal hydrogen atom of HO_2. These results may explain the faint OH($v = 10$) emission line recently detected in the night airglow[45] (see also ref 17). They may also support our recent suggestion[18] that vibrationally excited HO_2 radicals should be abundant in the middle atmosphere, since such species are formed when vibrationally excited OH radicals react with ozone.

Corresponding plots for the rotational quantum numbers are shown in Figures 6 and 7, with the characteristic attributes being gathered in Table 5. As seen, such distributions are rather similar for both DMBE surfaces, specially when looking to the values reported in Table 5 for the two lowest vibrational excitations of HO_2. The higher vibrational excitations lead both in the case of DMBEI and DMBEII to significantly higher values of $j^{\mathrm{OH}}_{\mathrm{max}}$ and $\langle j^{\mathrm{OH}} \rangle$, reflecting the change of mechanism pointed out in the previous paragraph. However, ignoring the many dips due to the small number of trajectories that would be necessary to run to get a smooth distribution, both the O_2 and OH rotational distributions do show some similarity with a Boltzmann distribution, and hence, we have calculated the corresponding averaged rotational temperatures by using $\langle E_{\mathrm{rot}} \rangle = k_{\mathrm{B}}T$. These

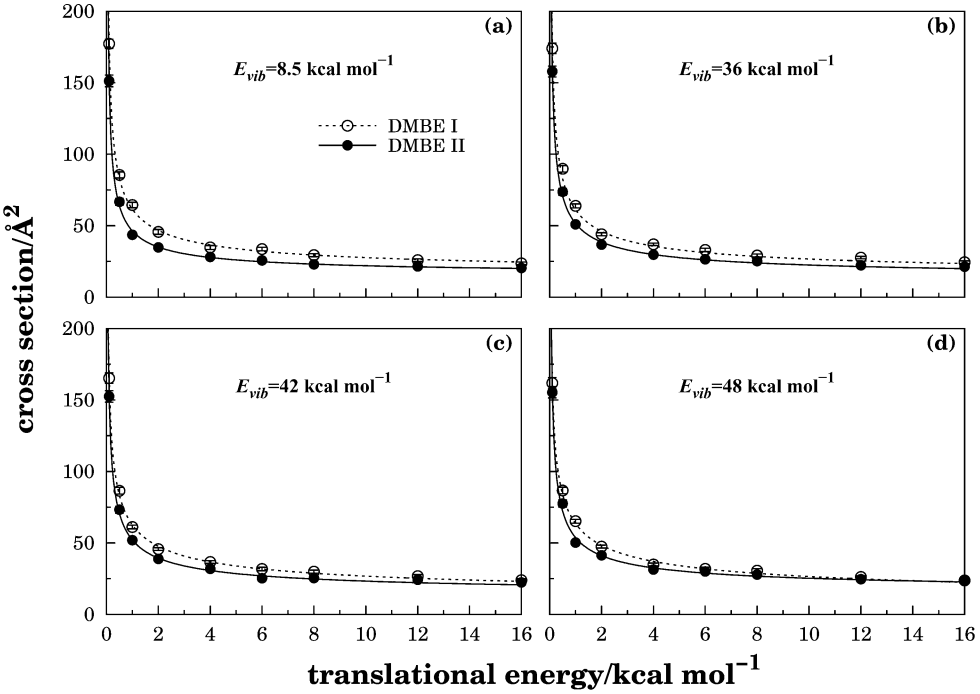

Figure 8. Calculated cross sections for the reaction O + HO_2 → OH + O_2 as a function of the translational energy and various initial vibrational energies of H_2O as obtained in the DMBEI potential energy surface. The lines indicate the fits based on eqs 9−11.

are summarized in Table 5, leading to average values of $T_{rot}^{O_2}$ = (5377 ± 480) K and T_{rot}^{OH} = (1768 ± 450) K for DMBEI; $T_{rot}^{O_2}$ = (5418 ± 250) K and T_{rot}^{OH} = (1556 ± 340) K for DMBEII. Also shown for comparison in Figures 6 and 7 are least-squares fits to normalized Boltzmann rotational distributions. Clearly, they suggest a roughly thermal rotational distribution in the products.

3.2.2. Reactive Cross Sections. Figure 8 shows, for the various initial vibrational excitations of HO_2, the calculated cross sections for the O + HO_2 reaction as a function of the translational energy as obtained from the DMBEI and DMBEII potential energy surfaces. The overall picture is that the calculated cross sections show, on increasing the collisional energy, a rapid decline at first and then a stabilization at high energies before reaching a plateau. Such a decreasing behavior with increasing collisional energy may be rationalized from the observation that the reaction is barrierless on both potential energy surfaces and hence one expects reaction to be dominated by capture through a long-range interaction potential of the form

$$V = C_n r^{-n} \tag{8}$$

where C_n is the effective long-range interaction (due to electrostatic, induction and dispersion forces, which are approximately described by both DMBEI and DMBEII) and r is the distance from the attacking oxygen atom to the center of mass of HO_2. This is a fair explanation, since the incoming O atom tends to attack the terminal oxygen atom of the triatomic molecule and the atom H is light (thus, the HO_2 molecule can easily rotate to offer the terminal O atom to the attacking one). Finally, for the high energy regime, one expects the leveling-off in the cross section to suggest a rigid spheres such as collision asymptote, i.e., the two interacting particles would see each other roughly as unpolarizable at high collisional energies. Naturally, one expects the effective radius of HO_2 to increase with initial vibrational energy, as indeed seems to be the case from the relative positioning of the asymptotic curves, especially for DMBEII.

TABLE 6: Numerical Parameters of Cross Section in Eqs 9−11

E_{vib} kcal mol^{-1}	n	C_n kcal mol^{-1}Å^n	η Å
	DMBE I		
8.5	3.73	44.04	2.10
36.0	3.76	47.02	1.99
42.0	4.32	107.89	1.59
48.0	4.68	193.83	1.19
	DMBE II		
8.5	3.14	13.45	2.16
36.0	3.53	26.41	1.93
42.0	3.66	30.18	1.95
48.0	3.59	27.11	2.14

To model the calculated cross sections, we have employed the form

$$\sigma^r = \sigma_{cap}^r + \sigma_{rsp}^r \tag{9}$$

where σ_{cap}^r accounts for the cross section due to capture of an oxygen atom from HO_2 and σ_{rsp}^r is a rigid spheres cross section that should be operative at high collisional energies. To represent the capture excitation function we have employed the form

$$\sigma_{cap}^r = n\pi(n-2)^{(2-n)/n}\left(\frac{C_n}{2E_{tr}}\right)^{2/n} \tag{10}$$

while the rigid spheres component is represented by

$$\sigma_{rsp}^r = \pi\eta^2 \tag{11}$$

with the coefficients C_n, n, and η being treated as adjustable parameters to be obtained from a least-squares fit to the calculated cross sections. As shown by the lines in Figure 8, the calculated cross sections are in essentially all cases fitted within their associated error bars (the optimum values of the least-squares fitting parameters are gathered in Table 6). The notable feature from this table is the small variation in the values

of n and η. For n, the fitted values may be rationalized from the observation that the leading long-range forces are those due to the electrostatic interaction of the permanent quadrupole moment of O(^3P) with the permanent dipole and quadrupole moments of OH. Based on the optimized atomic quadrupole moment model,[46,47] this would lead us to anticipate an attractive dependence on r^{-4} or r^{-5} for all angles of approach, respectively. Furthermore, one expects a further attractive contribution in r^{-6} from the leading induced-dipole induced-dipole dispersion interaction, with corresponding higher-order attractive contributions arising for subsequent terms in the dispersion expansion. In addition, contributions would arise from the induction energy, but this has not been explicitly included in the construction of the DMBEI and DMBEII potential energy surfaces. Since all such terms have the same sign, one is led to anticipate that their sum should vary as r^{-n}, with $n \leq 4$. Such an expectaction is corroborated in all cases for DMBEII and approximately for DMBEI, where for $E_{vib} = 42.0$ and 48.0 kcal mol^{-1} the values of n slightly exceed the value of 4. This may be attributed, at least partly, to remaining errors in the least-squares fit to the cross section data. Regarding the parameter η (effective hard-spheres ratio), it is seen to assume a value close to 2 Å except for the two DMBEI cases just referred. Such a result may be compared with the O···HO_2 van der Waals radius that may be estimated as the average of the O···O and HO_2···HO_2 van der Waals radii. Using van der Waals diameters for the homonuclear interactions of[48] $d_{O\cdots O} = 3.61$ Å and[49] $d_{HO_2\cdots HO_2} = 3.96$ Å, one gets $d_{O\cdots HO_2} = 3.79$ Å which is fairly close to the average (3.77 Å) of twice the values of η obtained for DMBEI ($2\eta = 3.44$ Å) and DMBEII ($2\eta = 4.09$ Å).

Finally, we need to address the effect of the initial vibrational excitation on the n and η parameters. First, the value of n is seen to increase with E_{vib} in the case of both DMBEI and DMBEII. This may be attributed to the average increase of size of the HO_2 radical with vibrational excitation and, hence, of the associated permanent dipole and quadrupole moments. A similar consideration could effectively be extended to the various polarizabilities, which would imply an increase on the value of the associated C_n dispersion coefficients. Unfortunately, the trends are not so clear for η. Although it is nearly constant and close to $\eta = 2$ Å in the case of DMBEII, its value is seen to decrease with increasing E_{vib} in the case of DMBEI. We believe that this is simply a consequence of a strong correlation between the n and η parameters during the least-squares fitting procedure. In fact, the largest deviations are associated to the two highest vibrational energy values where the anomalies in the values of n had already been pointed out. So, our tentative justification suggests a cancelation of errors in the least-squares fitting procedure (too large n values compensated by too small η ones), rather to any unambiguous physical effect.

3.2.3. Thermal Rate Coefficients. To calculate the thermal rate coefficient of the title reaction, we have used the following electronic degeneracy factor

$$g(T) = \frac{1}{5 + 3\exp(-227.6/T) + \exp(-325.9/T)} \quad (12)$$

which accounts for the electronic degeneracies of O(^3P) + HO_2($^2A''$) and the fact that the DMBE potential energy surface refers to HO_3(^2A).[11,33,50,51] By substitution of eqs 9−11 into eq 4, one obtains the analytical solution

$$k(T) = g(T)\left[\frac{2^{(3n-4)/2n} n\pi^{1/2}}{(n-2)^{(n-2)/n}\mu^{1/2}}\Gamma\left(\frac{2n-2}{n}\right)(k_B T)^{(n-4)/2n} C_n^{2/n} + \eta^2\pi\left(\frac{8k_B T}{\pi\mu}\right)^{1/2}\right] \quad (13)$$

where $\Gamma()$ is the gamma function, and all other parameters have the meaning assigned above. The rate constants calculated from eq 13 for temperatures over the range $100 \leq T/K \leq 500$ are shown in Figure 9. Each panel of this figure shows a comparison of the results obtained using DMBEI and DMBEII for a specific vibrational excitation of HO_2. It is seen that both surfaces, irrespective of E_{vib}, show the same general pattern as a function of temperature, as one might anticipate for a reaction occurring over a barrierless potential energy surface, i.e., controlled by long-range forces. The other visible fact refers to the value of the calculated rate constant which is predicted to be somewhat smaller in the case of DMBEII for all values of vibrational excitation considered in HO_2. This may be attributed to differences between the two surfaces which refer basically to the regions associated to the HO_3 intermediary and products channel, i.e., to regions where reaction has essentially already taken place. In fact, since the well depth associated with the stable HO_3 species is somewhat deeper in DMBEII than in DMBEI (specially if the well depth is measured up to the crest of the barrier that separates HO_3 from the OH + O_2 asymptote, i.e., 7.84 vs 1.50 kcal mol^{-1}), one can probably attribute the smaller reactivity of DMBEII to a higher probability that trajectories forming a HO_3 complex have to recross the centrifugal barrier back to O + HO_2 rather than yielding OH + O_2 products. In fact, a comparison of the nonreactive probabilities in Tables 2 and 3 show that they are generally significantly larger for DMBEII than for DMBEI, except for the highest value of E_{vib} where the difference tends to level-off or slightly increase at high collision energies.

The influence of the reactants vibrational excitation on the thermal rate coefficient is perhaps best seen from Figure 10, which shows by the shaded areas the range of calculated results for the various initial values of E_{vib}. Also included for comparison are the available experimental measurements,[2−8,8−10] the recommended values for the range $200 \leq T/K \leq 400$, and the results from our previous trajectory calculations.[11] The first significant observation refers to the small variation of $k(T)$ with vibrational excitation of HO_2. This is specially true for DMBEI, as indicated by the narrow band covered by the calculated rate constants for the four initial values of E_{vib} considered in the present work. In fact, even for DMBEII, the difference between $k(T)$ for the highest and smallest vibrational excitations of HO_2 does not exceed 10−20%. The other notable feature refers to the value of $k(T)$ obtained from DMBEII which is found to agree essentially within the error bars of the available experimental values. This is significant, since atmospheric modeling studies[14] have suggested that to get the best agreement with the observed densities of odd hydrogen in the atmosphere the recommended[15] rate coefficient should be scaled down by a factor up to 50−75%. The exception to the good agreement reported above seems to be the measurement at 1600 K, which significantly overestimates the DMBEII results and lies slightly above the DMBEI ones. As suggested elsewhere,[11] this may possibly be attributed to the opening of a channel not considered in the present work. In fact, we emphasize that nonadiabatic effects have been neglected in the present work, and these may turn out to be specially significant at high temperatures since there is the possibility of other electronic states becoming available. A final remark goes to the comparison between the results reported in

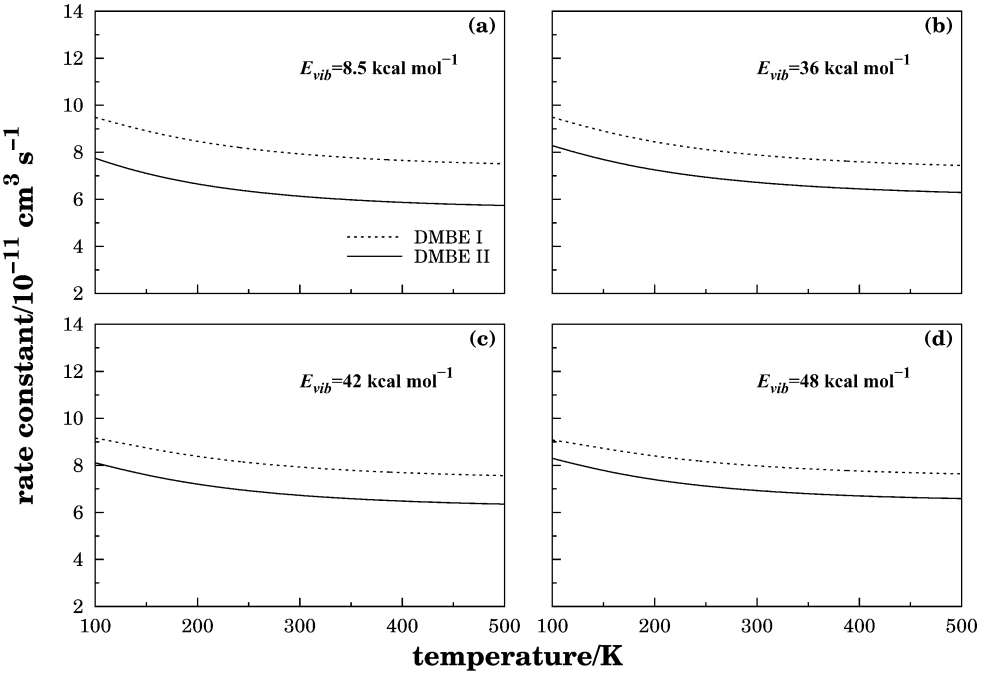

Figure 9. Thermal rate coefficients calculated from eq 13 for temperatures over the range 100 ≤ *T*/K ≤ 500. Each panel shows a comparison of the results obtained using the DMBEI and DMBEII potential energy surfaces for a specific vibrational excitation of the reactant hydroperoxyl radical.

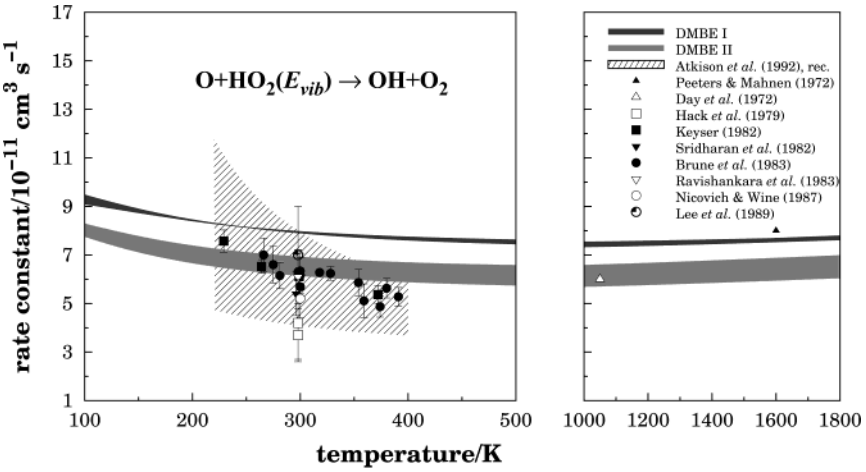

Figure 10. Influence of the reactants vibrational excitation on the thermal rate coefficient, and comparison with the available experimental measurements.[2−10]

this work for DMBEI and those previously reported[11] for the same potential energy surface. These are somewhat larger than the average values now reported for E_{vib} = 8.5 kcal mol^{-1}, which may be due to their poorer statistics. However, the two calculations essentially overlap within their associated error bars and hence can be said to be in good agreement with each other. In summary, there is good agreement (within 20% or so) between the two sets of theoretical results based on two DMBE potential energy surfaces and between these and the experimental results.

4. Conclusions

It has been recently suggested by one of us[16−18] that vibrationally excited species such as O_2, OH, and HO_2 could offer a clue to simultaneously explain the so-called "ozone deficit problem" (refs 16 and 19 and references therein) and the "HO_x dilemma",[20] which were pending in the literature for more than 15 years. Of special relevance in the theory was the observation that vibrationally excited hydroperoxyl radicals provide a nonconventional source of H atoms that might help to explain the partitioning of HO_x species into OH and HO_2. However, an important question that remained to be answered was how much the vibrational excitation of the hydroperoxyl radicals would affect the rate of title reaction, since this provides an important sink of ozone and hence which could then be enhanced via vibrational excitation of HO_2. The results of the prent work have shown that such an effect should be rather small even when considering HO_2 with contents of vibrational excitation (this has been partioned democratically by all vibrational normal modes) close to the H + O_2 dissociation asymptote. Thus, as advanced elsewhere,[18] such a vibrational excitation should not have implications in atmospheric modeling studies. Moreover, it does not affect the theory there proposed, where such an effect has actually been ignored. In fact, to the best of our knowledge, the explicit consideration of vibrationally excited HO_2 as an atmospheric entity has only recently been suggested[16−18] possibly because they are assumed to relax promptly in the middle atmosphere through collisions with

environmental species such as vibrationally cold oxygen and nitrogen molecules. To what extent this may happen is unknown at present, with studies along this direction being currently in progress in our group. Finally, the good agreement shown in Figure 10 between the rate constant calculated in the present work and its recommended[15] value as a function of temperature gives no clue for the need of drastically scaling it down in atmospheric modelling studies. Of course, some tolerable down-revision within the reported error bars cannot be ruled out.

Acknowledgment. This work has the financial support of Fundação para a Ciência e a Tecnologia, Portugal, via programs POCTI/40154/QUI/2001 and FEDER.

References and Notes

(1) Crutzen, P. *Science* **1997**, *277*, 1951.
(2) Peeters, J.; Mahnen, G. *Symp. (Int.) Combust.* **1972**, *14*, 133.
(3) Day, M. J.; Thompson, K.; Dixon-Lewis, G. *Symp. (Int.) Combust.* **1972**, *14*, 47.
(4) Hack, W.; Preuss, A. W.; Temps, F.; Wagner, H. *Ber. Bunsen-Ges. Phys. Chem.* **1979**, *83*, 1275.
(5) Lii, R. R.; M. C. Sauer, J.; Gordon, S. *J. Phys. Chem.* **1980**, *84*, 817.
(6) Nicovich, J. M.; Wine, P. H. *J. Phys. Chem.* **1987**, *91*, 5118.
(7) Keyser, L. F. *J. Phys. Chem.* **1982**, *86*, 3439.
(8) Sridharan, U. C.; Qiu, L. X.; Kaufman, F. *J. Phys. Chem.* **1982**, *86*, 4469.
(9) Ravishankara, A. R.; Wine, P. H.; Nicovich, B. M. *J. Chem. Phys.* **1983**, *78*, 6629.
(10) Brune, W. H.; Schwab, J. J.; Anderson, J. G. *J. Phys. Chem.* **1983**, *87*, 4503.
(11) Wang, W.; González-Jonte, R.; Varandas, A. J. C. *J. Phys. Chem.* **1998**, *102*, 6935.
(12) Varandas, A. J. C.; Szichman, H. *Chem. Phys. Lett.* **1998**, *295*, 113.
(13) Varandas, A. J. C. *Int. Rev. Phys. Chem.* **2000**, *19*, 199.
(14) Summers, M. E.; Conway, R. R.; Siskind, D. E.; Stevens, M. H.; Offermann, D.; Riese, M.; Preusse, P.; Strobel, D. F.; Russell, J. M., III. *Science* **1997**, *277*, 1967.
(15) Atkinson, R.; Baulch, D. L.; Cox, R. A.; Hampson, R. F., Jr.; Kerr, J. A.; Troe, J. *J. Phys. Chem. Ref. Data* **1992**, *21*, 1125.
(16) Varandas, A. J. C. *ChemPhysChem* **2002**, *3*, 433.
(17) Varandas, A. J. C. *J. Phys. Chem. A* **2003**, *107*, 3769.
(18) Varandas, A. J. C. *J. Phys. Chem. A* **2004**, *108*, 758.
(19) Miller, R. L.; Suits, A. G.; Houston, P. L.; Toumi, R.; Mack, J. A.; Wodtke, A. M. *Science* **1994**, *265*, 1831.
(20) Clancy, R. T.; Rusch, D. W.; Thomas, R. J.; Allen, M.; Eckman, R. S. *J. Geophys. Res.* **1987**, *92*, 3067.
(21) Speranza, M. *Inorg. Chem.* **1996**, *35*, 6140.
(22) Speranza, M. *J. Phys. Chem.* **1998**, *102*, 7535.
(23) Cacace, F.; de Petris, G.; Pepi, F.; Troiani, A. *Science* **1999**, *285*, 81.
(24) Cacace, F. Private communication, July 2001.
(25) Dupuis, M.; Fitzgerald, G.; Hammond, B.; Lester, W. A., Jr.; Schaefer, H. F., III. *J. Chem. Phys.* **1986**, *84*, 2691.
(26) Setokuchi, O.; Sato, M.; Matuzawa, S. *J. Phys. Chem. A* **2000**, *104*, 3204.
(27) Yu, H. G.; Varandas, A. J. C. *Chem. Phys. Lett.* **2001**, *334*, 173.
(28) Blint, R. J.; Newton, M. D. *J. Chem. Phys.* **1973**, *59*, 6220.
(29) Mathisen, K. B.; Gropen, O.; Skancke, P. N.; Wahlgren, U. *Acta Chem. Scand.* **1983**, *A37*, 817.
(30) Mathisen, K. B.; Siegbahn, P. E. M. *Chem. Phys.* **1984**, *90*, 225.
(31) Chen, M. M. L.; Wetmore, R. W.; Schaefer, H. F., III. *J. Chem. Phys.* **1981**, *74*, 2938.
(32) Vincent, M. A.; Hillier, I. H. *J. Phys. Chem.* **1995**, *99*, 3109.
(33) Varandas, A. J. C.; Yu, H. G. *Mol. Phys.* **1997**, *91*, 301.
(34) Nelander, B.; Engdahl, A.; Svensson, T. *Chem. Phys. Lett.* **2000**, *332*, 403.
(35) Yu, H. G.; Varandas, A. J. C. *J. Chem. Soc., Faraday Trans.* **1997**, *93*, 2651.
(36) Szichman, H.; Varandas, A. J. C. *J. Phys. Chem.* **1999**, *103*, 1967.
(37) Garrido, J. D.; Caridade, P. J. S. B.; Varandas, A. J. C. *J. Phys. Chem.* **1999**, *103*, 4815.
(38) Caridade, P. J. S. B.; Zhang, L.; Garrido, J. D.; Varandas, A. J. C. *J. Phys. Chem. A* **2001**, *105*, 4395.
(39) Varandas, A. J. C.; Caridade, P. J. S. B. *Chem. Phys. Lett.* **2001**, *339*, 1.
(40) Caridade, P. J. S. B.; Betancourt, M.; Garrido, J. D.; Varandas, A. J. C. *J. Phys. Chem. A* **2001**, *105*, 7435.
(41) Garrido, J. D.; Caridade, P. J. S. B.; Varandas, A. J. C. *J. Phys. Chem. A* **2002**, *106*, 5314.
(42) Hase, W. L., MERCURY: a general Monte Carlo classical trajectory computer program, QCPE#453. An updated version of this code is VENUS96: W. L. Hase, R. J. Duchovic, X. Hu, A. Komornik, K. F. Lim, D.-H. Lu, G. H. Peslherbe, K. N. Swamy, S. R. van de Linde, A. J. C. Varandas, H. Wang, R. J. Wolf, *QCPE Bull.* **1996**, *16*, 43.
(43) Weisman, M.; Shum, L. S. G.; Heneghan, S. P.; Benson, S. W. *J. Phys. Chem.* **1981**, *85*, 2863.
(44) Sridharan, U. C.; Klein, F. S.; Kaufman, F. *J. Chem. Phys.* **1985**, *82*, 592.
(45) Osterbrock, D. E.; Fulbright, J. P.; Cosby, P.; Barlow, T. A. *Publ. Astron. Soc. Pac.* **1998**, *110*, 1499.
(46) Varandas, A. J. C. *J. Mol. Struct. (THEOCHEM)* **1988**, *166*, 59.
(47) Varandas, A. J. C.; Brandão, J.; Quintales, L. A. M. *J. Phys. Chem.* **1988**, *92*, 3732.
(48) Hirschfelder, J. O.; Curtiss, R. F.; Bird, R. B. *Molecular Theory of Gases and Liquids*; Wiley: New York, 1954.
(49) Teitelbaum, H.; Caridade, P. J. S. B.; Varandas, A. J. C. *J. Chem. Phys.* **2004**, *120*, 10483.
(50) Langhoff, S. R.; Jaffe, R. L. *J. Chem. Phys.* **1979**, *71*, 1475.
(51) Johnson, B. R.; Winter, N. W. *J. Chem. Phys.* **1977**, *66*, 4116.